Available online at www.sciencedirect.com
SCIENCE DIRECT®
Microporous and Mesoporous Materials 60 (2003) 139–149
MICROPOROUS AND MESOPOROUS MATERIALS
www.elsevier.com/locate/micromeso

Pore structure and graphitic surface nature of ordered mesoporous carbons probed by low-pressure nitrogen adsorption

H. Darmstadt [a,*], C. Roy [a], S. Kaliaguine [a], S.H. Joo [b], R. Ryoo [b]

[a] *Department of Chemical Engineering, Laval University, Québec, Qc, Canada G1K 7P4*
[b] *National Creative Research Initiative Center for Functional Nanomaterials and Department of Chemistry (Center for Molecular Science-BK21), Korea Advanced Institute of Science and Technology, Daejeon 305-701, South Korea*

Received 6 November 2002; received in revised form 17 March 2003; accepted 21 March 2003

Abstract

Ordered mesoporous carbons (OMCs) were produced by pyrolysis of sucrose adsorbed in two different silica matrices (MCM-48 and SBA-15), followed by dissolution of the matrix in hydrofluoric acid. Subsequently, some of these OMCs were heat-treated at temperatures of up to 1600 °C. The OMC pore structure was studied by low-pressure nitrogen adsorption. Information on the graphitic order of the surface of the mesopore walls was also obtained from the nitrogen adsorption data. These results were correlated to the order of the graphene layers at the outer surface, which was studied by X-ray photoelectron spectroscopy (XPS).

The OMCs were predominantly mesoporous, but they also contained micropores. For OMCs produced in an SBA-15 matrix, the micropore volume decreased upon heating. After heating to 1600 °C, nearly all micropores had disappeared. Furthermore, upon heating the width of the mesopores increased from 35 to 50 Å. All these changes can be explained by a shrinking of the OMC framework upon heating. A different behavior was found for OMCs derived from MCM-48. Upon heating these materials at increasingly high temperatures, the width of the mesopores first decreased, and for temperatures above 1100 °C it increased again. For all OMCs studied the graphitic order of the mesopores and the order of the graphene layers at the outer surface increased upon heating. For a given temperature, the graphitic surface order of OMCs derived from SBA-15 and MCM-48 was similar.

Keywords: Mesoporous carbon; MCM-48; SBA-15; Nitrogen adsorption; Surface order

1. Introduction

Porous carbons such as activated carbon are important adsorbents and catalyst supports. Activated carbons are produced from various carbon-containing materials by pyrolysis/carbonization, followed by partial oxidation for activation. The pore structure of the activated carbons can be

* Corresponding author. Tel.: +1-418-656-2131x6931; fax: +1-418-656-2091.
E-mail addresses: hans.darmstadt@gch.ulaval.ca (H. Darmstadt), rryoo@mail.kaist.ac.kr (R. Ryoo).

1387-1811/03/$ - see front matter © 2003 Elsevier Science Inc. All rights reserved.
doi:10.1016/S1387-1811(03)00335-4

controlled to a certain degree by the carbonization and activation conditions. Carbon materials with uniform mesopores are highly desirable for the adsorption and catalytic transformation of large molecules. However, predominantly mesoporous activated carbons normally exhibit a broad distribution of mesopore widths [1,2]. A different synthesis approach has been developed in recent years, using the pyrolysis/carbonization procedure in a suitable matrix such as microporous zeolites [3–5] or mesoporous silicas [6]. In a second step of the synthesis, the carbon material is liberated by removal of the matrix, for example by treatment with hydrofluoric acid in the case of zeolite or silica matrices. Obviously, the structure of the produced carbon material can be controlled by the pore structure of the matrix or ''template''. The carbon materials obtained by the template-synthesis method usually have a narrow pore size distribution. A large-scale production of ordered mesoporous carbons (OMCs) by this approach should be possible since a convenient synthesis method for suitable mesoporous silicas was recently developed [7,8].

In the present work, the effect of heat treatments on the pore structure of the OMCs produced in MCM-48 and SBA-15 silica matrices, respectively, was investigated by nitrogen adsorption at −196 °C over a wide pressure range. The nitrogen adsorption data provide useful information on the graphitic order of the mesopore surface. The structural information on the pore-wall surface was compared with the structure of the outer surface, which was studied by X-ray photoelectron spectroscopy (XPS).

2. Experimental details

2.1. Materials

The OMCs were produced by pyrolysis of sucrose inside an MCM-48 [7] and an SBA-15 [9] silica matrix, respectively. Different pyrolysis experiments were performed at temperatures ranging from 700 to 1100 °C. After pyrolysis, the OMCs were liberated by dissolving the silica matrix in hydrofluoric acid solution. Some samples were subsequently heat-treated at temperatures ranging from 1100 to 1600 °C under vacuum or in purified nitrogen. The synthesis conditions of the OMCs are summarized in Table 1. For most OMC properties, the highest temperature during the synthesis (either during pyrolysis or the subsequent post-pyrolysis heat-treatment) was the determining parameter. Thus in the present work, generally it is not differentiated between the two heat-treatment procedures. However, in cases where the heat-treatment procedure had a significant influence this is mentioned. A non-porous thermal carbon black (SC N990) and a predominantly microporous activated carbon (Calgon F-

Table 1
Synthesis parameters of the OMCs

Sample	Silica matrix	Pyrolysis temperature (°C)	Post-pyrolysis heat-treatment temperature (°C)
CMK-3F(A)	SBA-15	700	–
CMK-3F(B)	SBA-15	900	–
CMK-3F(C)	SBA-15	900	1100[a]
CMK-3F(D)	SBA-15	900	1300[b]
CMK-3F(E)	SBA-15	900	1600[b]
CMK-1F(A)	MCM-48	700	–
CMK-1F(B)	MCM-48	900	–
CMK-1F(C)	MCM-48	900	1100[a]
CMK-1F(D)	MCM-48	1100	–
CMK-1F(E)	MCM-48	900	1300[b]
CMK-1F(F)	MCM-48	900	1600[b]

[a] Under vacuum.
[b] Under nitrogen.

300) were used as reference compounds. Information on the surface morphology and chemistry of the reference compounds can be found elsewhere [10–12].

2.2. Nitrogen adsorption

An Autosorb-1 MP apparatus from Quantachrome, Boynton Beach, FL, USA, was used for the nitrogen adsorption experiments at −196 °C. Prior to the adsorption experiments, samples of approximately 25 mg OMC were outgassed at 200 °C until the pressure increase in the closed sample cell was lower than 1.3 Pa/min. A typical final dynamic pressure was 0.13 Pa. The BET equation [13] was used to calculate the apparent surface area from data obtained at P/P_0 between 0.05 and 0.15. The cross sectional area of the nitrogen molecule was assumed to be 16.2 Å^2. The mesopore size distribution and the mesopore volume were calculated by the BJH method [14] using desorption data. It should be mentioned that the mesopores of the OMCs produced in the MCM-48 matrix were approximately 20 to 25 Å wide. The application of the BJH method to the adsorption data of materials with such narrow mesopores limits the precision of the results. Therefore, the widths of the mesopores of the OMCs produced in an MCM-48 matrix were only discussed qualitatively. The trends in pore width indicated by the BJH results were, however confirmed by results from the adsorption potential distribution (APD), which was calculated using the adsorption isotherm (see below). The combined volume of micro- and mesopores was calculated from the amount of nitrogen adsorbed at $P/P_0 = 0.95$ [15]. This calculation slightly overestimates the OMC pore volume since at $P/P_0 = 0.95$ a certain amount of nitrogen is also adsorbed on the outer surface.

The adsorption potential (A) is defined as the negative change of the Gibbs free energy of adsorption:

$$A = -\Delta G = -RT \ln(P/P_0) \quad (1)$$

where R is the gas constant, T the absolute temperature, and P/P_0 the relative pressure [16]. The APD is defined by the following equation:

$$APD = -(\Delta V / V_{\text{monolayer}})/\Delta A \quad (2)$$

where ΔV and ΔA are the differences in volume of adsorbed gaseous nitrogen [cm^3 STP/g] and in the adsorption potential, respectively, between two neighboring points of the adsorption isotherm, and $V_{\text{monolayer}}$ is the monolayer volume, determined from the APD (see Section 3.7, Table 2). Thus the APD is the negative derivative of the adsorbed

Table 2
Surface areas, pore volumes and pore widths of OMCs

Sample	Specific surface area (m^2/g)		Mesopore width[a] (Å)	Pore volume (cm^3/g)		
	BET	APD[b]		Mesopores		Micro- + Mesopores
				20–80 Å	20–500 Å	$P/P_0 = 0.95$
CMK-3F(A)	1721	(1320)[c]	35.0	1.18	1.25	1.53
CMK-3F(B)	1322	1080	44.5	1.16	1.23	1.42
CMK-3F(C)	1218	1040	47.0	1.04	1.18	1.34
CMK-3F(D)	1200	1018	49.0	1.16	1.23	1.36
CMK-3F(E)	837	727	50.5	0.98	1.04	1.15
CMK-1F(A)	1908	(1340)[c]	25.0	–	–	1.31
CMK-1F(B)	1609	(1080)[c]	24.0	–	–	1.16
CMK-1F(C)	1683	1102	21.0	–	–	1.07
CMK-1F(D)	1968	1344	21.0	–	–	1.26
CMK-1F(E)	1680	1326	24.5	–	–	1.07
CMK-1F(F)	1896	1473	24.5	–	–	1.26

[a] Maximum in the BJH pore size distribution.
[b] Adsorption potential distribution, see text for details.
[c] Approximation, see text for details.

volume nitrogen normalized to $V_{monolayer}$ with respect to A. The details of the XPS experiments can be found elsewhere [11].

3. Results and discussion

3.1. Nitrogen adsorption isotherms of OMCs produced in an SBA-15 matrix

The nitrogen adsorption isotherms of OMCs produced in MCM-48 [17] and SBA-15 [9] silica matrices, respectively, have already been described elsewhere. Briefly, the observed steep increase in adsorption on the OMCs produced in an SBA-15 matrix (series CMK-3F, see Table 1) for relative pressures (P/P_0) from 0.4 to 0.8 and the corresponding hysteresis loop are typical for materials with a narrow distribution of mesopore widths. The small adsorption for P/P_0 above 0.95, where multilayer formation takes place, indicates a small outer surface. It was furthermore concluded from nitrogen adsorption data that the non heat-treated OMCs contain micropores [9,17].

In the present investigation, it was observed that for OMCs produced in an SBA-15 matrix the isotherms changed considerably upon heat-treatment. First, the adsorption capacity decreased with increasing the heat-treatment temperature. This decrease was especially pronounced for very low relative pressures ($P/P_0 < 0.02$), where filling of micropores takes place. For higher P/P_0, where the filling of mesopores occurs, the decrease was much smaller (Fig. 1). This is a first indication that a significant portion of the micropores were "lost" during the heat-treatment at 1600 °C, whereas the volume of mesopores changed only little. Changes were also observed for the shape of the low-pressure portion of the isotherms, especially after heat-treatment at 1600 °C (sample CMK-3F(E), Fig. 2). This change is particularly noteworthy in relation to the decrease in micropore volume, while the shape of the low-pressure portion of the isotherm also depends on the graphitic order of the carbon surface [10,16,18]. The temperature dependence of these two properties will be discussed in detail below.

After the heat treatment, the hysteresis loop was shifted to higher P/P_0 with increasing the heat treatment temperature (Fig. 1). This shift indicates that the width of the mesopores increased during the heat treatment. The pore size analysis following the BJH algorithm revealed that the maximum of the mesopore size distribution shifted indeed from approximately 35 Å (CMK-3F(A)) to 50 Å (CMK-3F(E)) (Fig. 3). The mesopore size distribution became somewhat wider after the heat treatment, but pores wider than 80 Å were still negligible. Up to a heat-treatment temperature of

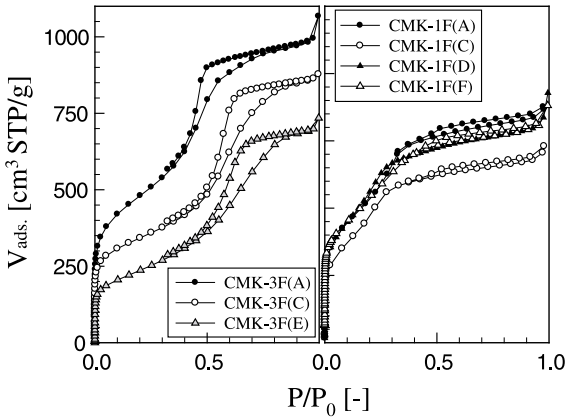

Fig. 1. Nitrogen adsorption isotherms at −196 °C for heat-treated OMCs produced in an SBA-15 (series CMK-3F) and MCM-48 (series CMK-1F) silica matrix, respectively.

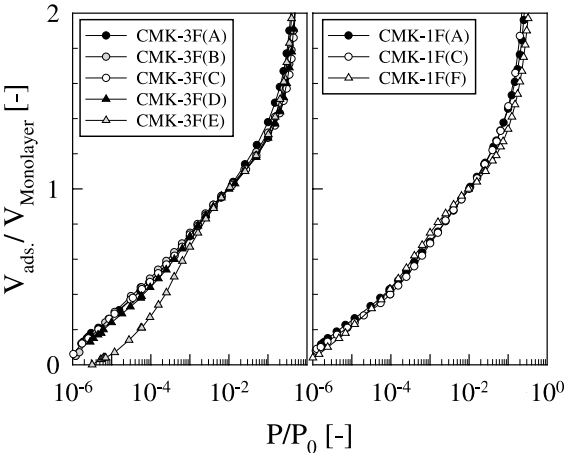

Fig. 2. Low-pressure nitrogen adsorption isotherms for heat-treated OMCs produced in an SBA-15 (series CMK-3F) and MCM-48 (series CMK-1F) silica matrix; normalized to the monolayer volume.

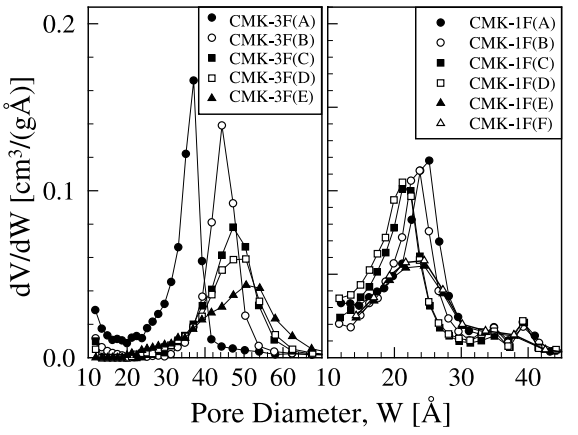

Fig. 3. Pore size distribution (mesopores) of heat-treated OMCs produced in an SBA-15 and an MCM-48 silica matrix, respectively; BJH method.

1300 °C (sample CMK-3F(D)), the total volume of the mesopores smaller than 80 Å changed very little (from 1.18 to 1.16 cm^3/g). However, the pore volume decreased to 0.98 cm^3/g when the temperature was further raised to 1600 °C (sample CMK-3F(E)) (Table 2).

3.2. Nitrogen adsorption isotherms of OMCs produced in an MCM-48 matrix

Similar to the CMK-3 OMCs obtained with SBA-15, the CMK-1 OMCs produced in the MCM-48 matrix have a mixed micro-/mesoporous structure. Nevertheless, the details of the adsorption isotherms were significantly different, as reported previously [17]. The total pore volume of CMK-1 was notably smaller than that of CMK-3, as compared under the same synthesis and treatment conditions (Fig. 1). The mesopore capillary condensation in CMK-1 occurred at lower pressures than those for CMK-3. This result, which is indicative of thinner mesopores of CMK-1, is consistent with thinner pore walls of the MCM-48 silica matrix. It is worth mentioning that the pore widths indicated by the BJH method extended well into the micropore region (width < 20 Å) (Fig. 3). However, considering that the BJH method normally underestimates the widths of the mesopores [8], the actual mesopore widths would be most probably larger than the values indicated in Fig. 3.

The data of the present investigation also show that the effects of heat-treatment were different between the OMCs produced in the two matrices. First, the changes of the isotherm upon heat-treatment were less pronounced for the OMCs produced in the MCM-48 matrix as compared to the OMCs produced in the SBA-15 matrix. Furthermore, with increasing heat-treatment temperature, there was a steady decrease in the amount adsorbed and a steady shift of the hysteresis to higher pressures for the OMCs produced in the SBA-15 matrix. On the other hand, for the OMCs produced in the MCM-48 matrix with increasing heat-treatment temperature, the amount of adsorption first decreased (samples CMK-1F(A) > CMK-1F(B) > CMK-1F(C)) and then increased again (samples CMK-1F(C) ~ CMK-1F(E) < CMK-1F(F)). A similar temperature dependence was observed for the mesopore widths. According to the BJH pore size distribution, the mesopores widths first decreased from approximately 25 Å (sample CMK-1F(A), 700 °C) to 21 Å (samples CMK-1F(C) and CMK-1F(D), 1100 °C) upon heating. Upon further temperature increases, the pore size distribution became wider and the maximum was shifted to approximately 24.5 Å (Fig. 3). The cause of these complex changes for CMK-1 seems to be related to the structural transformation, which takes place as the silica matrix is removed [9]. The structural transformation can be briefly described as follows: the structure of the MCM-48 mesoporous silica is composed of an enantiomeric pair of two separate three-dimensional channel systems, which produce two interpenetrating carbon networks. When the silica template is removed, these carbon networks are joined by their shifts along the (1 0 0) or (1 1 0) crystallographic axis in the cubic Ia3d structure [19,20]. The resulting structure belongs to the tetragonal $I4_1/a$ space group or the monoclinic $C2/c$. The contact between the carbon networks is believed to be weak. The weekly contacting structure of the CMK-1 OMC may be more sensitive to subsequent heat treatment than the rigidly retaining CMK-3 structure.

There are also indications that, in addition to the heat-treatment temperature, the synthesis procedure also had an important influence on the

structure of the OMCs. The highest temperature during the synthesis of the two samples CMK-1F(C) and CMK-1F(D) was 1100 °C. However, sample CMK-1F(D) was produced by pyrolysis at this temperature, whereas sample CMK-1F(C) was obtained by pyrolysis at 900 °C and a subsequent heat-treatment at 1100 °C (Table 1). In spite of the same highest temperature encountered by the two samples during their synthesis, there were pronounced differences in their pore structure. The surface area and the pore volume of sample CMK-1F(D) was considerably higher as compared to CMK-1F(C) (Table 2). This difference may also be relevant to the structural transformation mentioned above.

3.3. Adsorption potential distribution of OMCs produced in an SBA-15 matrix

As mentioned above, the nitrogen isotherms indicated that the micropore volume of OMCs produced in an SBA-15 matrix decreased upon heat-treatment. For porous carbons, such as activated carbons, the micropore volume can be determined from comparison plots such as t- or α-plots [21]. However, the presence of very narrow mesopores makes the determination of the micropore volume by comparison plots unreliable [17].

Thus, in the present investigation information on the development of the microporosity upon heat-treatment was extracted from the adsorption potential distribution (APD). The APD of carbon materials is influenced by the porosity and the structural order of the surface. As the easier case, first the APD of non-porous carbons is discussed. The APD of graphitized carbon blacks shows peaks at approximately 5.5, 3.0, and 0.7 kJ/mol [18]. These signals are attributed to the formation of the nitrogen monolayer, to a two-dimensional fluid-solid transition and to the second layer formation, respectively. With decreasing graphitic order of the carbon surface these peaks become wider and are shifted to lower adsorption potentials. Finally, the peaks for two-dimensional fluid-solid transition and the second-layer formation are disappearing. Thus, the APD of non-graphitized carbon blacks only shows a monolayer formation peak at 5.5 to 3.3 kJ/mol, depending on the graphitic order of the surface [10]. As an example the APD of the non-graphitized thermal carbon black SC N990 is presented in Fig. 4. The APD of this sample showed a monolayer formation peak at approximately 5.0 kJ/mol. Because of the relatively low graphitic order, the APD showed no indication of a two-dimensional fluid-solid transition or a second-layer formation peak.

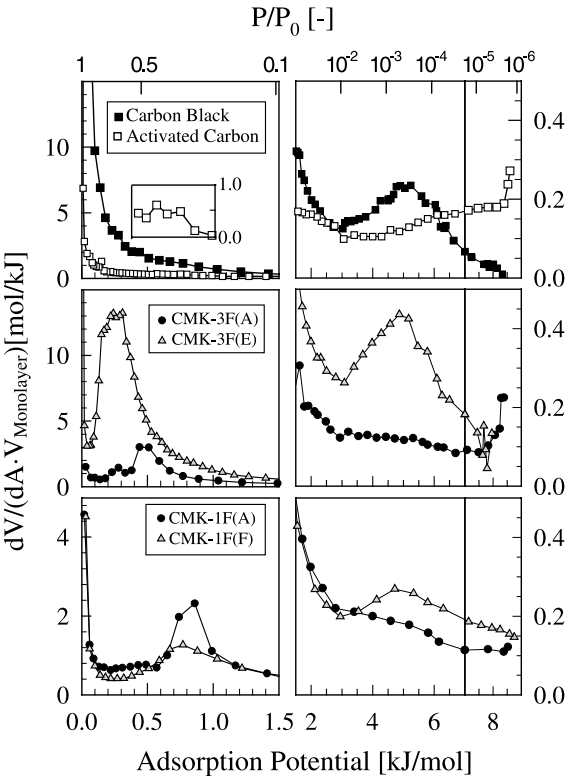

Fig. 4. Adsorption potential distributions for OMCs, non-porous carbon black SC N990 and predominantly microporous activated carbon (Calgon F300) normalized to the monolayer volume.

The presence of pores causes the appearance of additional peaks in the APD. In carbon materials the filling of very narrow micropores (width < 9 Å) occurs in one step, whereas in larger micro- and mesopores first a monolayer and then, depending on the pore size, additional layers are formed before the pores are filled [22]. Consequently, in the APD of carbons with very narrow micropores a one-step micropore filling peak is observed [23]. The one-step filling of the small micropores

(width < 9 Å) occurs at relative pressures below approximately 10^{-4} [22]. This pressure corresponds to an adsorption potential of approximately 6.0 kJ/mol. Consequently, in the APD the peak for one-step filling of narrow micropores is located at adsorption potentials above 6.0 kJ/mol. For carbon materials with pores wider than 9 Å, a monolayer formation and a secondary pore-filling peak are observed in the APD. Depending on the size of the pores, these two peaks may overlap.

As an example for a predominantly microporous activated carbon, the APD of Calgon F-300 is presented in Fig. 4. The APD showed a strong signal above an adsorption potential of 8.5 kJ/mol, indicating the presence of narrow micropores. The shoulder located between adsorption potentials of approximately 5–8.5 kJ/mol most probably contains contributions from the monolayer formation and secondary pore filling. Furthermore, there was a very weak peak at adsorption potentials between approximately 0.5–0.9 kJ/mol (Inset in Fig. 4), which indicates a small concentration of mesopores.

The discussion of the APD of the two reference compounds allows information to be obtained on the pore structure of the OMCs. The APD of sample CMK-3F(A) produced at 700 °C showed a strong signal at an adsorption potential of approximately 8.5 kJ/mol (Fig. 4). This is a clear indication for the presence of narrow micropores. The peak at approximately 0.5 kJ/mol is due to mesopore filling. The heat-treatment had a significant influence on the APD of the OMCs. In the APD of sample CMK-3F(E), heat-treated at 1600 °C, no signals due to small micropores were found at adsorption potentials above 6 kJ/mol. Instead, the APD approached zero for higher adsorption potentials. The APD of the OMC resembled those of the non-microporous carbon black SC N990. As for the carbon black, a pronounced peak at approximately 5 kJ/mol was observed. Theoretically, this peak could be assigned to larger micropores or the formation of the nitrogen monolayer. However, the creation of micropores during heat-treatment in nitrogen atmosphere or under vacuum is very unlikely. As discussed below, there are additional observations, which indicate that during the heat-treatment no micropores were formed. The micropore volume can be estimated from the difference of the combined volume of the meso- and micropores (calculated from the amount of nitrogen adsorbed at $P/P_0 = 0.95$) and the BJH mesopore volume (Table 2). These data indicate that the micropore volume of the OMCs strongly decreased during the heat-treatment. On the other hand, it is reasonable to assume that the heat-treatment increased the structural order of the surface. As discussed above, the APD of carbon materials with a certain order shows a monolayer formation peak. The peak at 5 kJ/mol was, therefore, assigned to the monolayer formation.

Another effect of the heat-treatment on the APD was that the mesopore filling peak was shifted to lower adsorption potentials, which reflects the widening of the mesopores, already observed in the BJH pore size distribution (Fig. 3). It can be concluded that upon heat-treatment of the OMCs produced in an SBA-15 matrix the initially present narrow micropores disappeared, whereas the mesopores became wider.

3.4. Adsorption potential distribution of OMCs produced in an MCM-48 matrix

As for the non-heat-treated OMC produced in an SBA-15 matrix (CMK-3F(A)), the APD of the corresponding OMC produced in an MCM-48 matrix (CMK-1F(A)) showed a strong signal at adsorption potentials above 6 kJ/mol (Fig. 4). This indicates that both samples contained narrow micropores. The effect of the heat-treatment on the narrow micropores, however, was different. For the OMCs produced in an SBA-15 matrix, the volume of the micropores decreased upon heat-treatment. Finally, after treatment at 1600 °C (nearly) all micropores have disappeared (see above). In all APDs of the heat-treated OMCs produced in an MCM-48 matrix strong signals were observed for adsorption potentials above 6 kJ/mol (only shown for sample CMK-1F(F) in Fig. 4). Thus, for these OMCs, the narrow micropores did not disappear upon heat-treatment. Even after heat-treatment at a temperature of 1600 °C the OMC still contained a significant concentration of narrow micropores. This conclusion is

supported by the observation that for very low P/P_0 the adsorption on the sample CMK-1F(A) (non-heat-treated) and on sample CMK-1F(F) (treated at 1600 °C) were very similar (Fig. 2).

As mentioned above, for the OMCs produced in an SBA-15 matrix, the micropore volume can be estimated by the difference of the nitrogen volume adsorbed at a relative pressure of 0.95 and the mesopore volume determined by the BJH method (Table 2). Unfortunately, this was not possible for the OMCs produced in an MCM-48 matrix, since for the narrow mesopores of these materials, the pore volume cannot be reliably calculated by the BJH method.

For the OMCs discussed here, the density functional theory (DFT) method is also not suitable since it assumes slit-like pores [24]. This may be a valid assumption for the micropores. The shape of the mesopores in the OMCs, however, most likely corresponds to the volume occupied by the silicon and oxygen atoms of the silica matrix and may be described as a three-dimensional network of roughly cylindrical pores. Because of the presence of both slit-like and cylindrical pores, models that are based on cylindrical pores exclusively [25] are also not applicable.

3.5. Graphitic surface order of the surface of OMCs

Information on the graphitic order of the surface can be obtained from the monolayer formation peak. As mentioned above, the position of the monolayer formation peak depends on the graphitic order of the carbon surface. For a series of graphitized carbon blacks a correlation between the bulk graphitic order, determined by X-ray diffraction, and the position of the monolayer formation peak was observed. With increasing graphitic order the monolayer formation peak was shifted to higher adsorption potentials [18].

It is reasonable to assume that during the heat-treatment the order of the OMC surface increases. Thus, upon heat-treatment, the monolayer formation peak in the APD is expected to shift to higher adsorption potentials. Exactly this behavior was observed in the present work for both series of heat-treated OMCs (Fig. 5). The APD of the

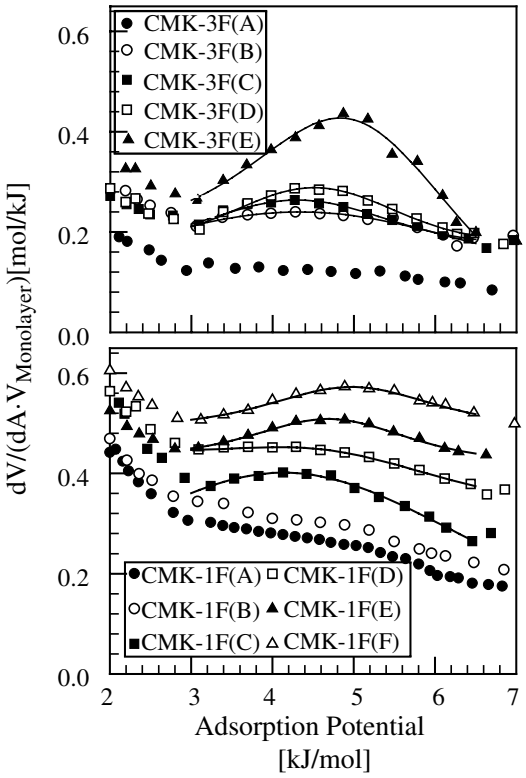

Fig. 5. Adsorption potential distribution for OMCs, monolayer formation peak.

OMCs produced in the SBA-15 matrix at 700 °C (sample CMK-3F(A)) showed no monolayer formation peak. However, after heating to 900 °C (CMK-3F(B)) a weak peak appeared at approximately 4.3 kJ/mol. Upon further heating the monolayer formation peak became more pronounced and was shifted to higher adsorption potentials. After heat-treatment at 1600 °C, the peak was located at an adsorption potential of approximately 5.0 kJ/mol (sample CMK-3F(E)).

For the OMCs produced in an MCM-48 matrix a similar temperature dependence of the position of the monolayer formation peak was observed. In fact, considering the uncertainty of the determination of the position of the rather wide monolayer formation peaks, the temperature dependence of the peak position was practically the same for the two series (Fig. 6). Since the pore structure of the OMCs produced in the two matrices differed considerably, this suggests that graphitic order

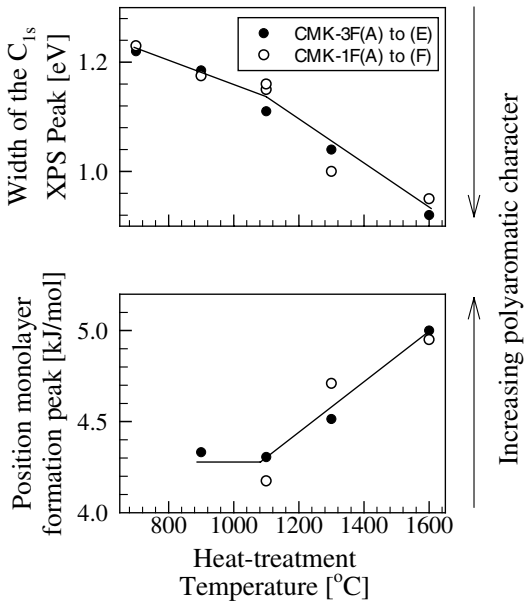

Fig. 6. Width of the XPS C_{1s} peak (measure for the polyaromatic character of the outer surface) and position of the monolayer formation peak (measure for the order of the mesopore surface) as a function of the heat-treatment temperature.

depends on the heat-treatment temperature and not or only very little on the pore structure.

During adsorption, the nitrogen monolayer is formed in the mesopores and on the outer surface of the OMC particles. However, as already mentioned, for the OMCs the outer surface was very small as compared to the mesopore surface. Thus, the position of the monolayer formation peak depends essentially on the order of the mesopore surface. It should be mentioned that the mesostructured carbon materials reported here constitute a very special case where the order of an internal surface can be studied by nitrogen adsorption. For the samples studied, the monolayer formation peak extended from adsorption potentials of approximately 3 to 6 kJ/mol (Fig. 5), corresponding to a P/P_0 range of approximately 10^{-4}–10^{-2}. At these pressures, when present, pores with widths between 9 and 12 Å are filled [22]. Only for carbon materials where the volume of such pores is very low, the monolayer formation in larger pores and the outer surface does not overlap with pore filling. Consequently, only for such carbon materials can one obtain information on the surface order from the nitrogen isotherms. Furthermore, if one is interested in properties of the mesopore surface the outer surface has to be small as compared to the surface of the mesopores. Unfortunately, these conditions are not met by most porous carbons. These materials usually contain micropores with widths between 9 and 12 Å. Thus, the analysis based on the low-pressure nitrogen isotherm presented here cannot be applied to "usual" porous carbons.

3.6. Comparison with surface spectroscopic results

It was outlined in the previous paragraph that for the samples studied it was possible to obtain information on the order of the mesopore surface from the low-pressure nitrogen adsorption data. In a parallel work [26], the polyaromatic character of the outer surface (plus the near surface region) of the same OMCs was studied by X-ray photoelectron spectroscopy (XPS). The most prominent signal in the carbon XPS spectra is the C_{1s} peak. The width of the C_{1s} peak strongly depends on the polyaromatic character of the carbon surface. The XPS spectra of highly polyaromatic, graphite-like carbons show a narrow C_{1s} peak, whereas much wider peaks are found for small polyaromatic compounds [27].

In Fig. 6 the full width at half maximum (FWHM) of the C_{1s} peak and the position of the monolayer formation peak in the APD, are plotted as a function of the heat-treatment temperature. With increasing temperature, the C_{1s} peak became narrower and the monolayer formation peak was shifted to higher adsorption potentials. This indicated that, both, the polyaromatic order of the outer surface and mesopores surface increased during the heat-treatment. The data indicate that for both outer and mesopore surface this increase was especially pronounced for temperatures above 1100 °C. Apparently, the development of a larger polyaromatic system upon heating on the outer and mesopore surface was similar. Another similarity between the XPS and nitrogen adsorption results was that for a given temperature the polyaromatic order of the surface of MCM-48 and SBA-15 based OMCs was similar.

3.7. Specific surface area of OMCs

The specific surface areas of the OMCs determined by the BET method were very large. BET surface areas of up to 1721 m^2/g were found (Table 2). Considering that the theoretical surface area of a single graphite layer is approximately 2630 m^2/g [22], the BET surface areas for the predominantly mesoporous OMCs are unrealistically high. The BET model does not consider adsorption in pores. It is well known that the BET model therefore often significantly overestimates the surface area of porous solids.

A more realistic value for the specific surface area can be obtained from the adsorption potential distribution (APD). For most of the samples studied, the APD showed a monolayer formation peak. The low adsorption potential end of the monolayer formation peak (minimum in the APD) indicates the point where the monolayer has been completed. From this point the volume of the nitrogen monolayer and the specific surface area can be calculated [16]. For the samples studied, the low adsorption potential end of the monolayer formation peak was located at an adsorption potential of approximately 3 kJ/mol (Fig. 5). This adsorption potential corresponds to a P/P_0 of approximately 10^{-2}. Therefore, the amount of nitrogen adsorbed at $P/P_0 = 10^{-2}$ was assumed to be the monolayer. The specific surface area was calculated from this amount. These APD surface areas were considerably lower than the corresponding BET surface areas (Table 2), which is more realistic for predominantly mesoporous OMCs. However, even the lower APD values indicate that the OMCs have the high surface areas required by a "good" adsorbent.

It should be mentioned, that there is some uncertainty in the determination of the end of the monolayer formation peak and consequently in the determination of the APD surface area. For activated carbons, however, the agreement between the surface areas calculated from the APD and by the DFT method was found to be usually better than 10% [16].

In the present work, for some OMC samples (CMK-3F(A), CMK-1F(A) and CMK-1F(B)), no monolayer formation peak was observed in the APD (Fig. 5). Therefore, for these samples the APD surface area calculated from the P/P_0 where the monolayer formation was completed for the other OMCs is only an approximation.

4. Conclusions

Carbon materials produced in SBA-15 and MCM-48 silica matrices are predominantly mesoporous. However, the materials also contain narrow micropores (width < 9 Å). For the OMCs produced in an SBA-15 matrix, the concentration of micropores decreases upon heating until at a temperature of 1600 °C a purely mesoporous material is obtained. Furthermore, the mesopore width increases from 35 to 50 Å. These changes can be explained as follows: The structure of the OMCs corresponds to the three-dimensional pore system of the SBA-15 silica, which may be visualized as interconnected carbon rods. During the heat-treatment, the carbon rods are shrinking and voids in the rods—the micropores—are disappearing. As the carbon rods become narrower, the space between them—the mesopores—becomes wider. The situation is different for the OMCs produced in an MCM-48 matrix. These materials contain, in addition to narrow micropores, small mesopores (width ≈ 25 Å). Upon heat-treatment, the mesopore width first decreases and then increases again. The narrow micropores do not disappear during the heat-treatment.

The OMCs have mesopore volumes and BET surface areas of up to 1.25 cm^3/g and 1700 m^2/g, respectively. Even if the BET surface areas are overestimated, the lower, but more realistic, surface areas calculated from the adsorption potential distributions (APD) of approximately 730–1400 m^2/g indicate that these materials have a high potential as adsorbents for large molecules and as catalyst supports. It should also be advantageous that for OMCs produced in an SBA-15 matrix the concentration of micropores can be influenced by the heat-treatment temperature.

The structural order of the outer and of the mesopore surface increases upon heat-treatment. In spite of the different structures of the OMCs produced in the two matrices, for a given tem-

perature the structural order of the outer and mesopores surface, respectively, was similar.

Acknowledgements

The authors are thankful to Dr. Annette Schwerdtfeger for reviewing the manuscript. R. Ryoo gratefully acknowledges that this work was supported in part by the Korean Ministry of Science and Technology through the Creative Research Initiative Program, and by the School of Molecular Science through the Brain Korea 21 Project.

References

[1] R.C. Bansal, J.-B. Donnet, F. Stoeckli, Active Carbon, Marcel Dekker Inc., New York, USA, 1988, p. 1.
[2] H. Jankowska, A. Swiatkowski, J. Choma, Active Carbon, Ellis Horwood, Chichester, UK, 1991, p. 75.
[3] T. Kyotani, T. Nagai, S. Inoue, A. Tomita, Chem. Mater. 9 (1997) 609–615.
[4] S.A. Johnson, E.S. Brigham, P.J. Olivier, T.E. Mallouk, Chem. Mater. 9 (1997) 2448–2458.
[5] J. Rodriguez-Mirasol, T. Cordero, L.R. Radovic, J.J. Rodriguez, Chem. Mater. 10 (1998) 550–558.
[6] R. Ryoo, S.H. Joo, S. Jun, J. Phys. Chem. B. 103 (1999) 7743–7746.
[7] R. Ryoo, S.H. Joo, J.M. Kim, J. Phys. Chem. B. 103 (1999) 7435–7440.
[8] M. Kruk, M. Jaroniec, R. Ryoo, S.H. Joo, Chem. Mater. 12 (2000) 1414–1421.
[9] S. Jun, S.H. Joo, R. Ryoo, M. Kruk, M. Jaroniec, Z. Liu, T. Ohsuma, O. Terasaki, J. Am. Chem. Soc. 122 (2000) 10712–10713.
[10] H. Darmstadt, C. Roy, Carbon 39 (2001) 841–848.
[11] H. Darmstadt, N.-Z. Cao, D.M. Pantea, C. Roy, L. Sümmchen, U. Roland, J.-B. Donnet, T.K. Wang, C.H. Peng, P.J. Donnelly, Rubber Chem. Technol. 73 (2000) 293–309.
[12] N.-Z. Cao, H. Darmstadt, C. Roy, Energy Fuels 15 (2001) 1263–1269.
[13] S. Brunauer, P.H. Emmet, E. Teller, J. Am. Chem. Soc. 60 (1938) 309–319.
[14] E.P. Barrett, L.G. Joyner, P.P. Halenda, J. Am. Chem. Soc. 73 (1951) 373–380.
[15] F. Rodriguez-Reinoso, M. Molina-Sabio, M.T. Gonzalez, Carbon 33 (1995) 15–23.
[16] M. Kruk, M. Jaroniec, K.P. Gadkaree, Langmuir 15 (1999) 1442–1448.
[17] M. Kruk, M. Jaroniec, R. Ryoo, S.H. Joo, J. Phys. Chem. B. 104 (2000) 7960–7968.
[18] M. Kruk, Z.J. Li, M. Jaroniec, W.R. Betz, Langmuir 15 (1999) 1435–1441.
[19] M. Kaneda, T. Tsubakiyama, A. Carlsson, Y. Sakamoto, T. Ohsuna, O. Terasaki, S.H. Joo, R. Ryoo, J. Phys. Chem. B 106 (2002) 1256–1266.
[20] L.A. Solovyov, V.I. Zaikovskii, A.N. Shmakov, O.V. Belousov, R. Ryoo, J. Phys. Chem. B 106 (2002) 12198–12202.
[21] S.J. Gregg, K.S.W. Sing, in: Adsorption, Surface Area, and Porosity, second ed., Academic Press, London, UK, 1982, p. 94.
[22] N. Setoyama, T. Suzuki, K. Kaneko, Carbon 36 (1998) 1459–1467.
[23] M. Kruk, M. Jaroniec, K.P. Gadkaree, J. Colloid Interface Sci. 192 (1997) 250–256.
[24] J.P. Olivier, Carbon 36 (1998) 1469–1472.
[25] A. Saito, H.C. Foley, AIChE J. 37 (1991) 429–436.
[26] H. Darmstadt, C. Roy, S. Kaliaguine, S. Choi, R. Ryoo, Carbon 40 (2002) 2673–2683.
[27] K. Morita, A. Murata, A. Ishitani, K. Muragana, T. Ono, A. Nakajima, Pure Appl. Chem. 58 (1986) 456–468.